

Z-scan method for nonlinear saturation intensity determination, using focused intense laser beams

Y. Albeck, D. M. Kandhasamy, and D. Strasser*

Institute of Chemistry, The Hebrew University of Jerusalem, 91904, Jerusalem, Israel

(Received 9 August 2014; published 20 November 2014)

We describe a method for determining saturation peak intensities of nonlinear intense field processes. The Z-scan method takes advantage of the balance between nonlinear response and interaction volume change as an intense laser pulse is focused onto a sample. We derive a robust geometric factor, directly relating the peak intensity at optimal target displacement from the focal plane and the corresponding saturation intensity. The Z-scan method allows obtaining saturation intensities with no need of *a priori* assumptions about the nonlinear process; surprisingly even for unfavorable finite depth samples. The method is demonstrated experimentally for an intense laser pulse interaction with molecular anions.

DOI: [10.1103/PhysRevA.90.053422](https://doi.org/10.1103/PhysRevA.90.053422)

PACS number(s): 33.80.Rv, 42.50.Ct, 33.80.Eh

I. INTRODUCTION

The study of intense laser interactions with matter has attracted significant experimental and theoretical attention [1–3]. The temporal compression of amplified laser pulses down to the femtosecond pulse durations leads, even at moderate focusing conditions, to peak field intensities exceeding the binding forces experienced by electrons inside atoms and molecules. Light matter interactions in this intense field regime were studied in atomic [4–7] and molecular systems [2,8–10] as well as in non-neutral cationic [11–13] and anionic [14–17] systems. Intense laser fields bring forth a variety of nonlinear phenomena, such as the ac stark-shift [18], bond softening [19,20], multiphoton ionization [2,21], above-threshold ionization [22], Coulomb explosion [23,24], and more [25–27]. In particular, studies of intense field processes opened an important pathway for attosecond technologies, based on an intuitive model developed to improve our quantitative understanding of the efficient intense field double-ionization process and provided a qualitative understanding of high-order harmonic generation by intense femtosecond laser pulses [28].

One of the experimental challenges is determining the peak intensity at which an intense field process of interest occurs. A specific difficulty arises from the intrinsically nonuniform intensity profile of a realistic laser beam focused on a finite sample volume [2,29,30]. At sufficiently high intensities nonlinear processes occur not only at the most intense center of a laser spot, but also at the larger volume of the rim of the spot where peak intensities are significantly lower. As strong interactions quickly saturate once all molecules at the most intense region have reacted, the majority of the nonlinear events of interest often occur at lower intensity regions, making it experimentally challenging to determine the peak intensity at which the nonlinear process of interest is measured. Various methods were proposed to limit the so-called volume effect, typically by drastically reducing the interaction volume and by implementing weaker focusing, resulting in relatively smaller signals from a uniform intensity region [30,31]. Furthermore, by evaluating the volume irradiated by intensities greater than some threshold intensity, attempts were made to retrieve the

underlying intensity dependence by weighing out the volume effect [29,30,32,33].

By careful examination of the volume effect Hankin *et al.* [34] have shown that considering a parallel Gaussian beam, the asymptotic dependence of an intense field process yield as a function of peak intensity logarithm provides information about the corresponding saturation intensity. Under realistic experimental conditions, laser beams are focused to reach the intense field regime. Therefore, the parallel beam requirement can be fulfilled at the focal plane, for very thin target depths below the Rayleigh length, where the peak intensity is systematically varied by reducing the total pulse energy.

Another efficient method for peak intensity variation is by displacement of a focusing element and moving the focal plane away from the target, a scheme often used in many cross-beam experiments and referred to as a “Z-scan” [11,33,35–40]. Z-scan measurements were previously analyzed to extract threshold intensities based by comparison to numerical simulations [37], assuming all atoms exposed to intensities above a certain threshold are ionized. However, the Z-scan results reported in the literature are often only qualitatively discussed without the extraction of quantitative data.

In this paper we describe a simple and robust method for the determination of saturation intensities of nonlinear intense field processes. The Z-scan measurement analysis presented here takes advantage of the balance between the nonlinear increase of product yield with decreasing z and the otherwise detrimental volume effect. Surprisingly, as we show in the following, the peak intensity reached at the z position maximizing product yield is directly related to the saturation intensity of the nonlinear process by an easily evaluated geometric factor. The detailed dependence of the geometric factor on the spatial and temporal characteristics of the laser pulse and its relatively negligible dependence on the nonlinearity of an *a priori* unknown process are discussed. Moreover, we show that reliable saturation intensities are obtained even using finite depth targets without drastically limiting the interaction volume. We demonstrate the power of the Z-scan method implemented in our experimental setup for the study of intense laser pulse interactions with molecular anions, allowing the simultaneous determination of saturation intensities for several multiple-detachment and dissociation processes.

*Corresponding author: strasser@huji.ac.il

II. Z-SCAN METHOD

The probability P to produce a photoproduct by a linear process can be generally described as

$$P \propto 1 - e^{-\frac{\sigma}{h\nu} \int I(t) dt}, \quad (1)$$

where σ is the cross section for the particular process, $h\nu$ is the photon energy, and $I(t)$ is the time-dependent instantaneous intensity. For a given particular temporal pulse shape it is comfortable to rewrite the probability in terms of the peak intensity I_0 and saturation intensity I_{sat} at which the probability reaches $(1 - \frac{1}{e})$ of its maximal value. We can then express the product yield of a process governed by a more general power law dependence on laser intensity as

$$\text{yield} \propto A(1 - e^{-(I_0/I_{\text{sat}})^n}), \quad (2)$$

where A is the target area irradiated by peak intensity I_0 . Both the beam area and peak intensity depend on the distance from the focal plane z . Assuming constant pulse energy and a flat intensity distribution over a round laser spot, the area scales with z^2 while the peak intensity has the inverse dependence scaling as z^{-2} . The two opposite trends lead to maximal yield at an optimal z_{max} displacement and a corresponding peak intensity I_{max} . While in the case of a linear process, characterized by $n = 1$, the maximal yield is reached with vanishing peak intensity covering a larger area, for nonlinear processes characterized by $n > 1$ intensity power dependence a maximal yield is reached at a finite z_{max} . By deriving the condition for a vanishing derivative of the yield with respect to z , i.e., $\text{yield}' = 0$ we can obtain the extremum z positions

$$z \left[1 - e^{-\left(\frac{I_{\text{max}}}{I_{\text{sat}}}\right)^n} \left(1 + n \left(\frac{I_{\text{max}}}{I_{\text{sat}}}\right)^n \right) \right] = 0. \quad (3)$$

The solution at $z = 0$ corresponds to the minimum yield observed at the focal point due to the vanishing interaction volume at the focal plane. As we show in the following, the same $z = 0$ minimum yield is obtained also when considering diffraction limited Gaussian beam focusing. Although the explicit analytical expression for the maximal yield at a finite z is nontrivial, I_{max} can always be written as

$$\frac{I_{\text{max}}}{I_{\text{sat}}} = G_n, \quad (4)$$

where G_n is a geometric factor that depends on the specific nonlinear intensity dependence of the process, as well as the spatial intensity profile. Using Eq. (3) it is possible to show that the geometric factor for a round flat top beam profile approaches the asymptotic value of unity at the limit of infinite n , $\lim_{n \rightarrow \infty} (G_n) = 1$, i.e., the maximum yield is obtained at a z displacement corresponding to the saturation intensity.

To explore the explicit dependence of the geometric factor on n we solved Eq. (3) numerically up to $n = 20$. The blue circles in Fig. 1(a) show the dependence in the simplified case of a flat intensity profile. A maximal value of $G_n = 1.2$ is obtained for $n = 3$ and then rapidly approaches the asymptotic value of unity from above. The empty green squares show the geometric factor for a more realistic Gaussian intensity profile, calculated by integrating over the yield from the entire target area. It can be expected that a nonuniform intensity profile exhibits a higher geometric factor compared to a uniform

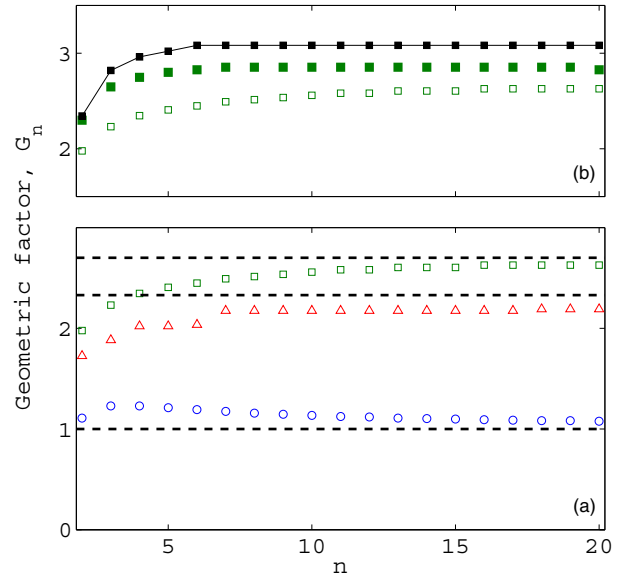


FIG. 1. (Color online) (a) The n dependence of the geometric factor that relates I_{max} and I_{sat} , simulated for square (blue circles), Gaussian (empty green squares), and sinc² (red triangles) pulses, calculated with a flat top temporal profile. (b) Comparing Geometric factors calculated for Gaussian beam profile and flat top (empty squares) and Gaussian (full squares) temporal pulse shapes. Square markers with full line shows calculation considering also a finite target depth of $3.5 \times z_r$.

flat profile since the lower intensity areas will saturate at stronger focusing thus shifting the balance between the volume effect and nonlinear intensity dependence to higher I_{max} . As expected, the resulting geometric factor for $n = 2$ reaches a value of 2 and converges rapidly towards an asymptotic value of 2.7, reaching 2.4 already for $n = 5$. As shown in Fig. 1(a) the overall dependence on n is surprisingly weak, thus no additional knowledge of the exact nonlinear response of the yield is required to determine the saturation intensity with $\sim 15\%$ uncertainty. To illustrate the robust nature of the method we performed numerical calculations of the geometric factor also for a sinc² like intensity profile. Again, as shown in Fig. 1(a) since the low intensity tail of a sinc² decays slightly faster than the tail of a Gaussian profile, the geometric factors derived for a sinc² beam profile are $\sim 15\%$ lower with a similarly weak n dependence rapidly converging to a value of 2.3. We tested further the robustness of our assumptions, numerically calculating the geometric factor dependence on the exact time-dependent shape assumed for $I(t)$, comparing rectangular flat top pulses to more realistic Gaussian and sech² pulse shapes while maintaining fixed total power and temporal FWHM. As could be expected, the gradual rise of the realistic pulse shapes results in a slight increase of up to $\sim 15\%$ in the computed geometric factor for low n values, becoming less significant with increasing n (opposite to the n dependence calculated for realistic beam profiles). Thus, for the typical Gaussian beam profile and Gaussian temporal pulse shape we obtain the weak n dependence shown by the full squares in Fig. 1(b), rapidly converging to the asymptotic value of 2.8. Similar results were obtained for sech² pulses with equivalent FWHM.

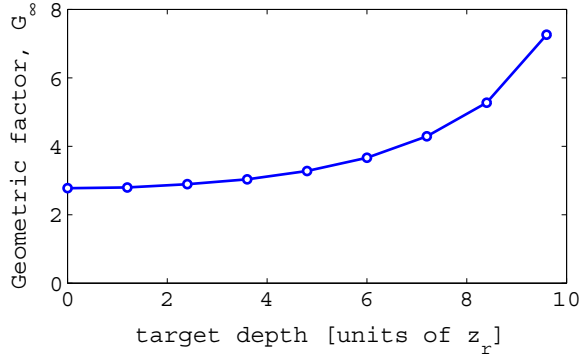


FIG. 2. (Color online) The effect of a realistic target depth on the asymptotic geometric factor, simulated for a spatial and temporal Gaussian pulse shape.

In a realistic experimental scenario one also has to consider the finite target depth, i.e., its extension along the Z-scan axis. We performed detailed numerical simulations including our typical experimental signal to noise ratios, realistic beam profile, and temporal 35-fs pulse shape as well as the change of the Gaussian beam waist along the extended 5-mm target depth, according to

$$w(z) = w_0 \sqrt{1 + \left(\frac{z}{z_r}\right)^2}, \quad (5)$$

with a $z_r \sim 1.5$ mm Rayleigh length and a $w_0 \sim 22$ μ m minimal beam waist at the focal plane. The full line with full square marker in Fig. 1(b) shows the resulting geometric factor n dependence taking into account all the experimental parameters of the spatial beam profile, focusing conditions, temporal pulse shape, and finite target depth. We obtain an asymptotic geometric factor of 3 and up to 7% systematic error for low-order nonlinear processes. The geometric factor is expected to grow with the extending target depth as the balance shifts towards tighter focusing and higher I_{\max} . Figure 2 shows the geometric factor correction that increases with increasing target depth, calculated for high n values. Surprisingly, for a target depth as large as 3.5 times the Rayleigh length the geometric factor is systematically increased by only $\sim 10\%$, while even $5 \times z_r$ target depth deviates by less than 15%.

To illustrate the Z-scan analysis, Fig. 3 shows selected Z-scan simulations, performed assuming $n = 2, 4$, and 10; Figs. 3(a) and 3(b) show calculations made with I_{sat} values of 10^{13} and 10^{14} W/cm², respectively. The clearly visible minimum yield at vanishing z values is in fact an important experimental marker allowing *in situ* determination of the $z = 0$ offset point, even if a direct measurement of the beam waist at the interaction region is physically impossible. The dashed lines indicate the z_{\max} positions. The systematic dependence of z_{\max} and corresponding I_{\max} on the saturation intensity is clearly visible, with a tighter focusing required to maximize the higher I_{sat} process, and only weak dependence on n .

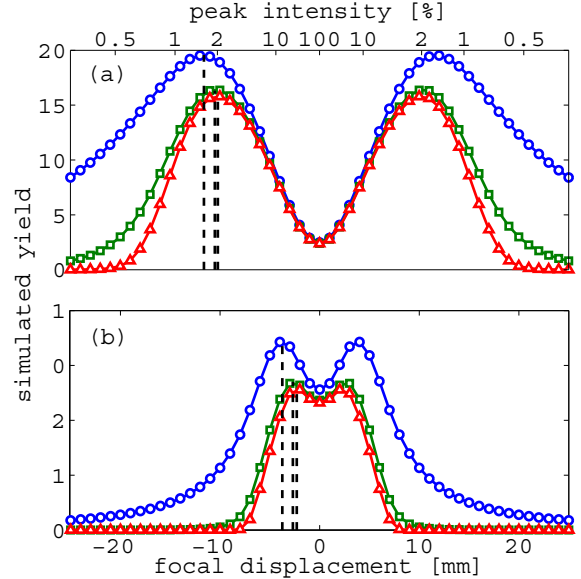


FIG. 3. (Color online) Simulated yield from Z scan for selected nonlinear orders $n = 2$ (blue circles), $n = 4$ (green squares), and $n = 10$ (red triangles). Panels (a) and (b) show simulations performed for $I_{\text{sat}} = 10^{13}$ and 10^{14} W/cm², respectively. The dashed lines indicate I_{\max} position illustrating the relatively small effect of an *a priori* unknown n .

III. EXPERIMENTAL SETUP

Figure 4 shows a schematic representation of our experimental setup for the study of intense laser interactions with molecular and cluster ions, previously described in Ref. [17]. Briefly, cold molecular and cluster anions of interest are generated in a pulsed supersonic expansion Even-Lavie ion source [41]. Typically, ~ 200 eV electrons are directed at the expanding gas mixture of $\sim 99\%$ argon carrier gas and $\sim 1\%$ traces of precursor sample gas. After passing a differential pumping section anions are accelerated to 4.6 keV by a set of pulsed Wiley-McLaren electrodes towards the photofragment spectrometer. Ions of interest are mass selected based on their time of flight by the “mass gate” (vertical deflector electrodes located at the entrance of the photofragment spectrometer between two grounded shield electrodes). The top and bottom deflector electrodes are supplied with opposite ± 750 V potentials achieving a well-localized electric field that is switched off for ~ 1 μ s by two synchronized high-voltage switches to allow selected ions to pass. Selected ions are then collimated by 5-mm diameter apertures and accelerated by an additional 3-kV potential applied to the photofragment spectrometer with a uniform gradient between the entrance electrode and the field free interaction region. In the interaction region the ion beam is intersected by the optical path of a focused intense laser beam. After passing through the interaction region anions are decelerated, while neutral products formed in the interaction region continue with the same velocity and cationic products are further accelerated by the photofragment spectrometer potential. The parent anions, neutral, and cationic products separate according to their charge over mass ratio along a 0.61-m flight before reaching a time and position sensitive microchannel plate (MCP) detector. As indicated in Fig. 4, an

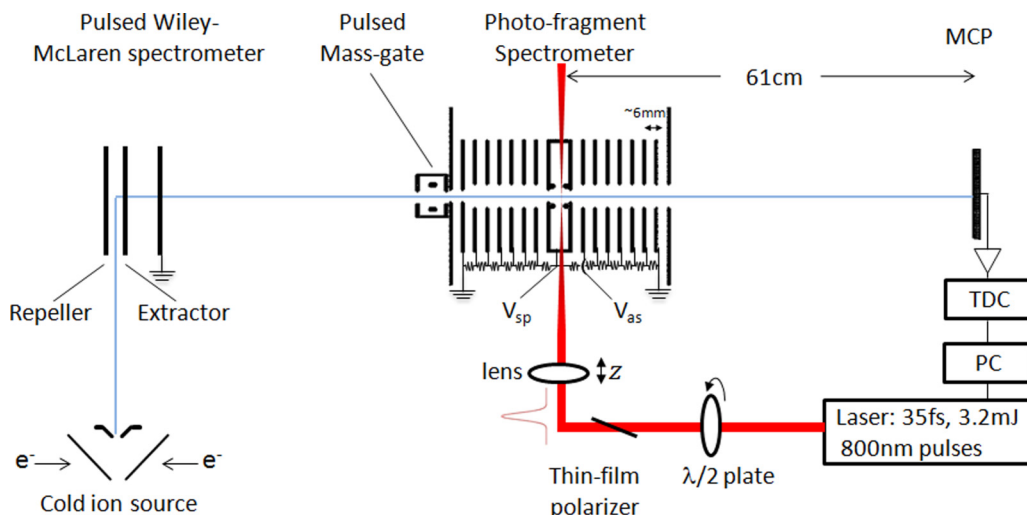


FIG. 4. (Color online) Experimental setup scheme.

“asymmetric” 3.8 keV potential is applied to one electrode to suppress a parasitic cation background on the detector due to intense field ionization of the residual gas in the interaction region, achieved with minimal trajectory distortions to cations formed in the moving frame of the parent anion beam. A computer-controlled time delay between the opening of the mass-gate and laser pulse allows either to synchronize the fs laser pulse with the ns ion bunch, or alternatively to intentionally miss and carefully characterize the parasitic background signals. In the experiments described here only the time of flight (TOF) information, recorded by a multithit time-to-digital-converter, is analyzed to retrieve the product yields and demonstrate the Z-scan method. Figure 5 shows a typical background subtracted SF_6^- photofragment spectrum produced by amplified 800 nm, 35 fs linearly polarized ~ 3

mJ laser pulses, focused by a 250 mm focal length lens and reaching peak intensities of up to $2.7 \times 10^{15} \text{ W/cm}^2$. The early TOF peaks are assigned to multiply charged atomic F^{2+} , S^{3+} , and S^{2+} cations arriving, respectively, at 2.5, 2.7, and $3.3 \mu\text{s}$ after the laser passes through the interaction region. The next TOF peaks arrive at 3.3 and $4 \mu\text{s}$ and correspond to singly charged F^+ and S^+ cations, respectively, followed by the molecular SF_n^+ cation spectrum. Neutral product TOFs are not mass resolved, arriving at $\sim 6.5 \mu\text{s}$ and parent anions arrive at $\sim 8.5 \mu\text{s}$ TOF (not shown).

In a Z-scan measurement, the yields of different products are recorded as a function of lens position displacement using a computer-controlled translation stage. In a typical measurement procedure, peak intensities are scanned over two orders of magnitude by focal point displacement from negative to positive z displacements and back in steps of 1 mm, collecting both signal and background TOF spectra for ~ 5000 laser shots at each z displacement. The Z-scan is typically repeated a few hundred times until a satisfactory signal to noise ratio is obtained. We also examine the explicit peak intensity dependence of product yields, measured at fixed focusing conditions. In these measurements the laser beam power is systematically attenuated by a computer-controlled rotation of a half wave plate in front of a thin film polarizer, allowing continuous tuning of laser peak intensity without modification of the temporal pulse shape.

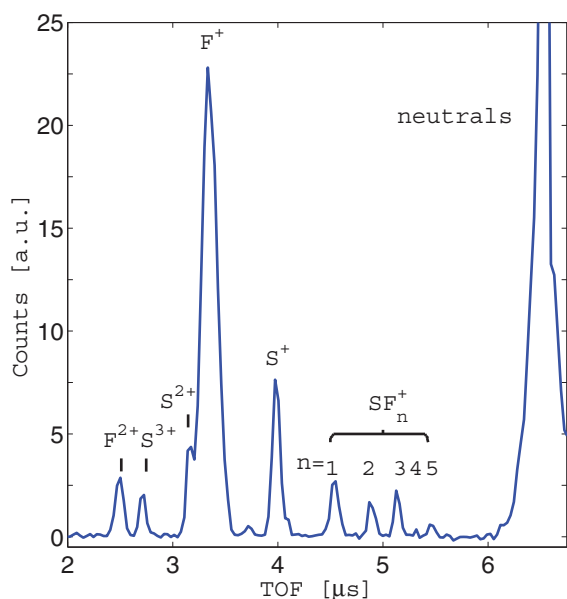


FIG. 5. (Color online) Typical background subtracted photofragment TOF spectrum showing single, double, and multiple dissociative detachment products. TOFs are measured relative to the laser pulse timing.

IV. EXPERIMENTAL RESULTS AND DISCUSSION

Figure 6 shows the relative yields of neutral products, singly charged molecular cations, and singly and multiply charged atomic products resulting from intense laser interactions with SF_6^- ions, measured as a function of a Z-scan and the corresponding peak intensities. The vertical detachment energy, required for the removal of a single electron from the SF_6^- anion is $\sim 3 \text{ eV}$ [42–45]. The appearance energy of molecular cations due to the dissociative ionization of neutral SF_6 is significantly higher, from 15.3 eV for the production of the SF_5^+ cation up to the 31-eV SF^+ appearance energy [46,47]. Complete fragmentation into atomic F^+ and S^+

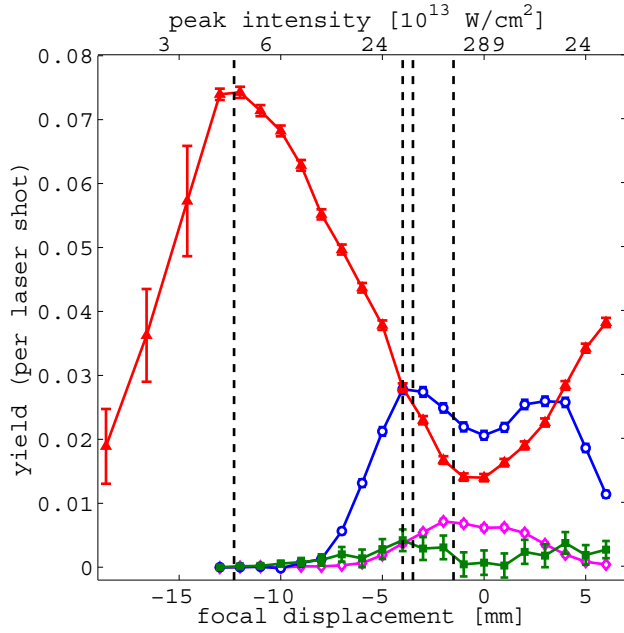


FIG. 6. (Color online) Z-scan yield profile of the different photodetachment products: neutrals (red full triangles), atomic cations (blue open circles), molecular cations (green full squares), and multiply ionized fragments (magenta open diamonds). The maxima relate to the balance between intensity and volume effects and are found to occur at different z_{\max} displacements of 12, 4, 3.5, and 1.5 mm corresponding to I_{\max} intensities of 0.4, 4, 6, and 18×10^{14} W/cm² for neutrals, molecular cations, atomic cations, and multiply ionized products, respectively.

corresponds to even higher 37- and 38-eV appearance energies, respectively [46]. The second and third ionization energies of the sulfur atom each require an additional 10.4 and 23.3 eV, respectively [48]. The second ionization energy of the fluorine atom is 17.4 eV, while the F^{3+} cation that was not observed in our spectra requires an additional 35 eV [48]. Given these vast differences in appearance energies, one expects to find a strong systematic trend in the corresponding saturation intensities. Table I lists the derived saturation intensities based on the measured I_{\max} and asymptotic geometric factor of 3 for the multiple detachment processes and $G_2 = 2.35$ for the two-photon single detachment process. It should be noted that the main source of error estimated in Table I and increasing with increasing I_{sat} does not stem from the Z-scan method approximations, but from the uncertainty in the estimated absolute peak intensities that are increasingly sensitive to

TABLE I. Saturation intensities for different photoproducts derived by a Z scan and by the method Hankin *et al.* use, contrasted by estimated appearance energies (AE) relative to the anion precursor.

	Neutrals	Molecular cations	Atomic cations	Multiply charged
estimated AE [eV]	~3	18–34	40–41	50.4–63.3
$I_{\text{sat}} [10^{13} \text{ W/cm}^2]$	1.7 ± 0.3	14 ± 6	19 ± 9	59 ± 30
$\tilde{I}_{\text{sat}} [10^{13} \text{ W/cm}^2]$	2.5 ± 0.5	36 ± 19	34 ± 9	

the absolute $z = 0$ position uncertainty in this measurement. In principle, finer Z-scan steps would enable reducing the absolute I_{sat} uncertainties down to the $\sim 15\%$ uncertainty in the geometric factor imposed by the *a priori* unknown nonlinear response. Nevertheless, the relative saturation intensities measured simultaneously in a single Z-scan are significantly more robust as processes reaching maximal yield closer to the focal plane saturate at correspondingly higher peak intensities. Indeed, cation species production are found to saturate at peak intensities that are an order of magnitude higher than the saturation intensity derived for neutral production, while even higher intensities are needed to saturate the production of multiply ionized atoms. However, the difference between the saturation intensities derived for molecular and atomic cations are much smaller despite the significant difference in the corresponding appearance energies. We interpret the apparent discrepancy of the I_{sat} and appearance energy trends to be due to the particular highly efficient intense field mechanism for multiple detachment from a molecular anion system [17]. It is possible that efficient excitation to high-lying potential curves prior to dissociation result in directly competing channels for atomic and molecular cation production, which are hence similar in saturation properties. Further studies investigating this discrepancy are on their way.

As mentioned in the Introduction, Hankin *et al.* [34] implemented an alternative method for the determination of the saturation intensities based on an analysis of the asymptotic linear dependence of the product yield curve as a function of peak intensity logarithm. Assuming a parallel beam or alternatively a vanishing target depth as well as a Gaussian shape of the laser beam, Hankin *et al.* [34] showed that in the limit of strong saturation the product yield converges to a linear dependence on the peak intensity logarithm of the form

$$\text{yield}(I) \propto \ln(I_0) - \ln(\tilde{I}_{\text{sat}}). \quad (6)$$

For a nonlinear power-law dependence \tilde{I}_{sat} , as it is defined by Hankin *et al.* [34,49], is directly related to I_{sat} as defined in Eq. (2) converging to the exact I_{sat} value at the high n limit.

For a Gaussian pulse shape the $I_{\text{sat}}/\tilde{I}_{\text{sat}}$ ratio follows $\sqrt{\frac{2\eta}{4n \ln(2)}} \frac{\pi e^{2\gamma}}{4n \ln(2)}$, where γ is Euler's constant, yielding a ratio of 1.15 for $n = 2$ and rapidly converging to unity.

Figure 7 shows the measured intensity dependencies of neutrals, atomic as well as molecular cation products, recorded during measurement periods comparable to the Z-scan measurements. Note that due to the finite dynamic range of the ability to attenuate laser power without affecting the temporal pulse shape, the measurements were performed at two different z offsets.

The \tilde{I}_{sat} saturation intensities fitted from the asymptotic yield dependence on intensity according to Eq. (6), as proposed by Hankin *et al.*, are listed in Table I. Although fitted \tilde{I}_{sat} values are found to agree within the experimental errorbars with the absolute I_{sat} saturation intensities obtained from Z-scan data, an overall shift towards higher intensities is evident. As the asymptotic yield dependence used in the \tilde{I}_{sat} fit is intrinsically more sensitive to the target regions sampled by lower peak intensities, the systematic shift can be tentatively explained by the finite target depth. Numeric simulations including the finite target effect indicate 25%-35%

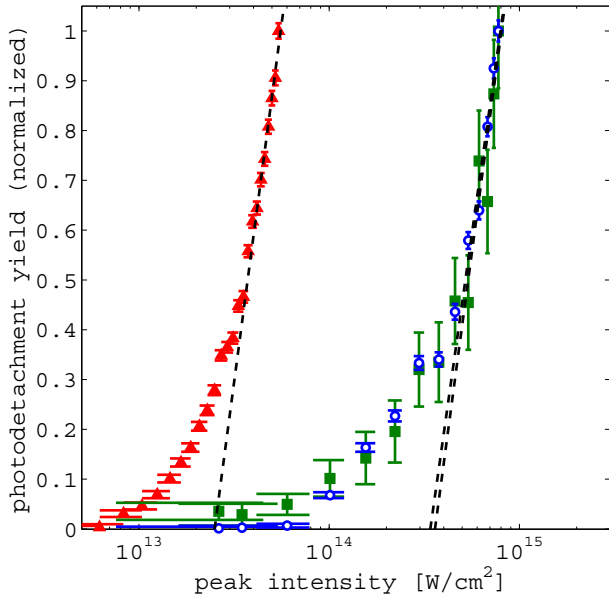


FIG. 7. (Color online) Intensity dependencies of neutral (red triangles), as well as cationic atomic (blue circles) and molecular (green full squares) products. Saturation intensities are defined by asymptotic linear fits, providing $\tilde{I}_{\text{sat}} = 2.5 \times 10^{13} \text{ W/cm}^2$ for neutralization and almost indistinguishable $\tilde{I}_{\text{sat}} = 36$ and $34 \times 10^{13} \text{ W/cm}^2$ for producing molecular and atomic cations, respectively.

\tilde{I}_{sat} overestimation, depending on assumed n , due to the deviation from the parallel beam approximation; thus accounting for the systematic shift of \tilde{I}_{sat} values in Table I. In addition to the uncertainty of absolute intensities, the ambiguity in the asymptotic region contributes to the higher \tilde{I}_{sat} errorbars, particularly for the molecular cations fit. The errorbars reported in Table I were determined by systematically changing the asymptotic range fitted with a linear curve, thus reflecting also the sensitivity of the model to the nonperfect Gaussian mode of our laser beam ($M^2 \approx 1.75$). In fact, a multiply charged species yield, measured for peak intensities up to $8 \times 10^{14} \text{ W/cm}^2$ is found to be insufficient for the reliable determination of the asymptotic dependence on peak intensity.

V. CONCLUSION

A robust method for determining saturation intensities of nonlinear intense field processes was derived from a Z-scan analysis of product yields as a function of displacement of the focal plane from a finite depth target. Saturation intensities are determined based on the balance between the nonlinear product yield dependence on peak intensity and the otherwise detrimental volume effect. The geometric factor, relating saturation intensities to the I_{max} peak intensity at z_{max} displacement of maximal product yield can be numerically estimated for any given laser beam characteristics. Moreover, it is found to be

only weakly dependent on the model assumptions such as the explicit nonlinear yield dependence on pulse intensity, temporal pulse shape, and exact beam profile. Most surprisingly, the method allows the extraction of reliable saturation intensities even under unfavorable extended target depths, making it particularly suitable for low-target density samples.

The method is implemented in our experimental setup, demonstrating a simultaneous saturation intensity measurement for several product channels of intense field interaction with molecular anions. Indeed, the characterization of complex competing processes with comparable rates by saturation intensities is subject to higher-order effects. For example, early quenching of the less efficient process can result in its effective I_{sat} attenuation. Similarly, product depletion by sequential processes [30,36,38] with similar saturation may shift I_{sat} of the initial product to lower values due to the rise of a secondary process. In this paper we demonstrate the Z-scan method measuring saturation intensities spanning two orders of magnitude for SF_6^- nonlinear single and nonsequential [17] multiple photodetachment processes. Nevertheless, the method is not limited to ion-laser interaction measurements and is well suited for practically any intense field experiment, examining the interaction with a finite depth target.

The obtained saturation intensities are compared to saturation intensities measured implementing the previously proposed method employing a peak intensity scan at constant focusing conditions. In contrast to the intensity scan method requiring a well-controlled attenuation of ultrafast pulses over a high dynamic range without affecting their temporal pulse shape, the Z-scan method relies on the intrinsic peak intensity variation as a laser beam approaches the focal plane. Thus allowing reliable systematic peak intensity variation over several orders of magnitude without introducing additional optical elements that may distort the temporal ultrafast pulse shape. In general, the analysis of the asymptotic product yield relies heavily on the nearly parallel analytic Gaussian beam profile, while the Z-scan method presented here can be implemented using even low-quality beam profiles with minimal adjustments made to the numerically evaluated geometric factor, taking into account an actual beam profile measurement, exact pulse shape, and extended target depth effects. The robust derivations presented here will allow the extraction of valuable quantitative data from the Z-scan measurement procedure, routinely performed in many cross-beam intense laser field experiments.

ACKNOWLEDGMENTS

The authors gratefully acknowledge funding from the European Community's seventh framework [FP7/2007-2013] under Grant No. 247471, as well as from the Legacy Heritage Fund (Israel Science Foundation) and the Minerva James-Frank program. We also acknowledge the assistance of Professor Ori Cheshnovsky of Tel-Aviv University who provided us with the cold ion source system as well as valuable knowhow.

[1] M. Protopapas, C. H. Keitel, and P. L. Knight, *Reports Prog. Phys.* **60**, 389 (1997).

[2] J. H. Posthumus, *Reports Prog. Phys.* **67**, 623 (2004).

- [3] W. Becker, X. Liu, P. J. Ho, and J. H. Eberly, *Rev. Mod. Phys.* **84**, 1011 (2012).
- [4] A. L'Huillier, L. A. Lompre, G. Mainfray, and C. Manus, *Phys. Rev. Lett.* **48**, 1814 (1982).
- [5] A. L'Huillier, L. A. Lompre, G. Mainfray, and C. Manus, *Phys. Rev. A* **27**, 2503 (1983).
- [6] B. Walker, E. Mevel, B. Yang, P. Breger, J. P. Chambaret, A. Antonetti, L. F. DiMauro, and P. Agostini, *Phys. Rev. A* **48**, R894(R) (1993).
- [7] A. Rudenko, K. Zrost, B. Feuerstein, V. L. B. de Jesus, C. D. Schröter, R. Moshhammer, and J. Ullrich, *Phys. Rev. Lett.* **93**, 253001 (2004).
- [8] C. Guo, M. Li, J. P. Nibarger, and G. N. Gibson, *Phys. Rev. A* **58**, R4271 (1998).
- [9] M. Lezius, V. Blanchet, M. Y. Ivanov, and A. Stolow, *J. Chem. Phys.* **117**, 1575 (2002).
- [10] I. V. Hertel and W. Radloff, *Reports Prog. Phys.* **69**, 1897 (2006).
- [11] V. S. Prabhudesai, U. Lev, A. Natan, B. D. Bruner, A. Diner, O. Heber, D. Strasser, D. Schwalm, I. Ben-Itzhak, J. J. Hua, B. D. Esry, Y. Silberberg, and D. Zajfman, *Phys. Rev. A* **81**, 023401 (2010).
- [12] M. Zohrabi, J. McKenna, B. Gaire, N. G. Johnson, K. D. Carnes, S. De, I. A. Bocharova, M. Magrakvelidze, D. Ray, I. V. Litvinyuk, C. L. Cocke, and I. Ben-Itzhak, *Phys. Rev. A* **83**, 053405 (2011).
- [13] J. McKenna, A. M. Sayler, B. Gaire, N. G. Johnson, K. D. Carnes, B. D. Esry, and I. Ben-Itzhak, *Phys. Rev. Lett.* **103**, 103004 (2009).
- [14] J. Pedregosa-Gutierrez, P. A. Orr, J. B. Greenwood, A. Murphy, J. T. Costello, K. Zrost, T. Ergler, R. Moshhammer, and J. Ullrich, *Phys. Rev. Lett.* **93**, 223001 (2004).
- [15] B. Bergues and I. Y. Kiyani, *Phys. Rev. Lett.* **100**, 143004 (2008).
- [16] A. Gazibegović-Busuladžić, D. B. Milošević, W. Becker, B. Bergues, H. Hultgren, and I. Y. Kiyani, *Phys. Rev. Lett.* **104**, 103004 (2010).
- [17] Y. Albeck, D. M. Kandhasamy, and D. Strasser, *J. Phys. Chem. A* **118**, 388 (2014).
- [18] P. J. Bustard, G. Wu, R. Lausten, D. Townsend, I. A. Walmsley, A. Stolow, and B. J. Sussman, *Faraday Discuss.* **153**, 321 (2011).
- [19] P. H. Bucksbaum, A. Zavriyev, H. G. Muller, and D. W. Schumacher, *Phys. Rev. Lett.* **64**, 1883 (1990).
- [20] B. Sheehy and L. F. DiMauro, *Annu. Rev. Phys. Chem.* **47**, 463 (1996).
- [21] G. Mainfray and C. Manus, *Reports Prog. Phys.* **54**, 1333 (1991).
- [22] P. Agostini, F. Fabre, G. Mainfray, G. Petite, and N. K. Rahman, *Phys. Rev. Lett.* **42**, 1127 (1979).
- [23] K. Sattler, J. Mühlbach, O. Echt, P. Pfau, and E. Recknagel, *Phys. Rev. Lett.* **47**, 160 (1981).
- [24] Th. Fennel, K.-H. Meiwes-Broer, J. Tiggesbäumker, P.-G. Reinhard, P. M. Dinh, and E. Suraud, *Rev. Mod. Phys.* **82**, 1793 (2010).
- [25] T. Zuo and A. D. Bandrauk, *Phys. Rev. A* **52**, R2511(R) (1995).
- [26] I. A. Bocharova, R. Karimi, E. F. Penka, J.-P. Brichta, P. Lassonde, X. Fu, J.-C. Kieffer, A. Bandrauk, I. V. Litvinyuk, J. Sanderson, and F. Légaré, *Phys. Rev. Lett.* **107**, 063201 (2011).
- [27] J. Eden, *Prog. Quantum Electron.* **28**, 197 (2004).
- [28] P. B. Corkum, *Phys. Rev. Lett.* **71**, 1994 (1993).
- [29] P. Wang, A. M. Sayler, K. D. Carnes, B. D. Esry, and I. Ben-Itzhak, *Opt. Lett.* **30**, 664 (2005).
- [30] P. Hansch, M. A. Walker, and L. D. Van Woerkom, *Phys. Rev. A* **54**, R2559(R) (1996).
- [31] A. Talebpour, C. -Y. Chien, and S. L. Chin, *J. Phys. B* **29**, 5725 (1996).
- [32] G. N. Gibson, R. R. Freeman, T. J. McIlrath, and H. G. Muller, *Phys. Rev. A* **49**, 3870 (1994).
- [33] T. R. J. Goodworth, W. A. Bryan, I. D. Williams, and W. R. Newell, *J. Phys. B* **38**, 3083 (2005).
- [34] S. M. Hankin, D. M. Villeneuve, P. B. Corkum, and D. M. Rayner, *Phys. Rev. Lett.* **84**, 5082 (2000).
- [35] P. Hansch, M. A. Walker, and L. D. Van Woerkom, *Phys. Rev. A* **57**, R709(R) (1998).
- [36] L. Robson, K. W. D. Ledingham, P. McKenna, T. McCanny, S. Shimizu, J. M. Yang, C. -G. Wahlstrom, R. Lopez-Martens, K. Varju, P. Johnsson, and J. Mauritsson, *J. Am. Soc. Mass Spectrom.* **16**, 82 (2004).
- [37] T. Döppner, J. P. Müller, A. Przystawik, S. Göde, J. Tiggesbäumker, K. -H. Meiwes-Broer, C. Varin, L. Ramunno, T. Brabec, and T. Fennel, *Phys. Rev. Lett.* **105**, 053401 (2010).
- [38] M. Schultze, B. Bergues, H. Schröder, F. Krausz, and K. L. Kompa, *New J. Phys.* **13**, 033001 (2011).
- [39] S. G. Sayres, M. W. Ross, and A. W. Castleman, Jr., *Phys. Chem. Chem. Phys.* **13**, 12231 (2011).
- [40] A. A. A. El-Zein, P. McKenna, W. A. Bryan, I. M. G. Johnston, T. R. J. Goodworth, J. H. Sanderson, I. D. Williams, W. R. Newell, P. F. Taday, E. J. Divall, and A. J. Langley, *Phys. Scr.*, **T 92**, 119 (2001).
- [41] U. Even, J. Jortner, D. Noy, N. Lavie, and C. Cossart-Magos, *J. Chem. Phys.* **112**, 8068 (2000).
- [42] G. L. Gutsev and R. J. Bartlett, *Mol. Phys.* **94**, 121 (1998).
- [43] W. Eisfeld, *J. Chem. Phys.* **134**, 054303 (2011).
- [44] P. G. Datskos, J. G. Carter, and L. G. Christophorou, *Chem. Phys. Lett.* **239**, 38 (1995).
- [45] J. C. Bopp, J. R. Roscioli, M. A. Johnson, T. M. Miller, A. A. Viggiano, S. M. Villano, S. W. Wren, and W. C. Lineberger, *J. Phys. Chem. A* **111**, 1214 (2007).
- [46] A. P. Hitchcock and M. J. Van der Wiel, *J. Phys. B* **12**, 2153 (1979).
- [47] M. Sasanuma, E. Ishiguro, T. Hayashida, H. Masuko, Y. Morioka, T. Nakajima, and M. Nakamura, *J. Phys. B* **12**, 4057 (1979).
- [48] J. H. Sanderson, R. V. Thomas, W. A. Bryan, W. R. Newell, P. F. Taday, and A. J. Langley, *J. Phys. B* **30**, 4499 (1997).
- [49] S. M. Hankin, D. M. Villeneuve, P. B. Corkum, and D. M. Rayner, *Phys. Rev. A* **64**, 013405 (2001).